JOURNAL OF SPACECRAFT AND ROCKETS
Vol. 36, No. 3, May–June 1999

Ablation and Thermal Response Program for Spacecraft Heatshield Analysis

Y.-K. Chen* and Frank S. Milos†
NASA Ames Research Center, Moffett Field, California 94035-1000

An implicit ablation and thermal response program is presented for simulation of one-dimensional transient thermal energy transport in a multilayer stack of isotropic materials and structure that can ablate from a front surface and decompose in depth. The governing equations and numerical procedures for solution are summarized. Solutions are compared with those of an existing code, CMA, and also with arcjet data. Numerical experiments show that the new code is numerically more stable and solves a much wider range of problems compared with the older code. To demonstrate its capability, applications for thermal analysis and sizing of aeroshell heatshields for planetary missions of Stardust, Mars Microprobe (Deep Space II), Saturn Entry Probe, and Mars 2001, using advanced lightweight ceramic ablators developed at NASA Ames Research Center, are presented and discussed.

Nomenclature

a = absorption coefficient, m^{-1}
B' = dimensionless mass blowing rate, $\dot{m}/\rho_e u_e C_M$
B_a = pre-exponential constant in Eq. (8), s^{-1}
C_H = Stanton number for heat transfer
C_M = Stanton number for mass transfer
c_p = specific heat, J/kg-K
E_a = activation temperature in Eq. (8), K
F = view factor
g = outward pyrolysis mass flux, kg/m^2-s
h = enthalpy, J/kg
$\bar{h}$ = partial heat of charring, defined in Eq. (6), J/kg
I' = radiation source function in Eq. (2), W/m^2-sr
i^+ = radiant intensity in $+x$ direction, W/m^2-sr
i^- = radiant intensity in $-x$ direction, W/m^2-sr
K = extinction coefficient, $a + \sigma_s$, m^{-1}
k = thermal conductivity, W/m-K
$\dot{m}$ = mass flux, kg/m^2-s
P = pressure, N/m^2
q_C = conductive heat flux, W/m^2
q_R = radiative heat flux, W/m^2
R = universal gas constant, J/kmol-K
s = surface recession, m
$\dot{s}$ = surface recession rate, m/s
T = temperature, K
u = velocity, m/s
x = moving coordinate, $y - s$, m
y = stationary coordinate, m
Z^* = coefficient in Eq. (9), defined in Ref. 10
α = surface absorptance
Γ = volume fraction of resin
ε = surface emissivity
θ = time, s
κ = optical thickness
κ_D = optical thickness for path of length D
λ = blowing reduction parameter
ρ = density, kg/m^3
σ = Stefan–Boltzmann constant, W/m^2-K^4
σ_s = scattering coefficient, m^{-1}
τ = mass fraction of virgin material, defined in Eq. (5)
Ψ = decomposition reaction order in Eq. (8)

Subscripts

c = char
e = boundary-layer edge
g = pyrolysis gas
i = density component (A, B, and C)
j = surface species
v = virgin
w = wall

Received Jan. 5, 1998; presented as Paper 98-0273 at the AIAA 36th Aerospace Sciences Meeting, Reno, NV, Jan. 12–15, 1998; revision received Aug. 15, 1998; accepted for publication Feb. 22, 1999.

*Aerospace Engineer, Thermal Projection Materials and Systems Branch, MS 234-1.
†Aerospace Engineer, Thermal Projection Materials and Systems Branch. Senior Member AIAA.

Introduction

SPACECRAFT heatshields typically use thermal protection system (TPS) materials that pyrolyze and ablate at high temperature for mass-efficient rejection of aerothermal heat load. Pyrolysis is an internal decomposition of the solid that releases gaseous species, whereas ablation is a combination of processes that consume heatshield surface material. For design and sizing of ablating spacecraft TPS materials, it is imperative to have a reliable numerical procedure that can compute surface recession rate, in-depth pyrolysis, and internal temperature histories under general heating conditions.

The program[1] CMA was developed by the Aerotherm Corporation in the 1960s. It solved the internal energy balance and decomposition equations coupled with the ablating surface energy balance condition to simulate the response of ablative heatshields in hypersonic flows. Since then, the CMA code has been widely used in the aerospace industry for analysis of ablating TPS materials on re-entry vehicles and space probes. However, in the CMA code, the in-depth energy equation is linked explicitly to the internal decomposition and ablating surface equations, and the decomposition rate is computed with an explicit method.[2] Thus, CMA solutions are sensitive to the user-specified time step as well as to grid size, and the solution accuracy is difficult to estimate. If the pyrolysis gas rate or the surface recession rate is sufficiently high, CMA computations can fail to converge because of the nature of the explicit scheme implemented in the code.

Recently a methodology for high fidelity TPS sizing computations[3,4] for hypersonic vehicles was developed at NASA Ames Research Center. This procedure relies on iterations between a flow environment code and a TPS thermal response code. This iteration process is computationally intensive, and any numerical instability, such as that which can occur in CMA, will substantially slow down or thwart the entire iteration process. To streamline this iterative procedure, an accurate and numerically stable thermal response code is indispensable.

This work presents the program[5] FIAT, which is a reliable and stable numerical procedure for simulation of thermal response of ablators for spacecraft heatshields under a wide range of surface and in-depth conditions. In addition to removing the potential numerical instability problem of the CMA code, the FIAT code has additional new features such as an integrodifferential equation for internal radiative flux, optimized TPS thickness, and a flow code interface. FIAT and CMA solutions for test cases are compared to verify the code consistency and accuracy. The predicted in-depth temperature histories for phenolic-impregnated carbon ablator[6] (PICA) and silicone-impregnated reusable ceramic ablator[7] (SIRCA) are compared with data from arcjet tests. Results from analysis of advanced lightweight ceramic ablators developed at NASA Ames Research Center, such as PICA and SIRCA with and without secondary impregnation, for the space missions of Stardust, Mars 2001 (Ref. 8), Mars Microprobe, and a Saturn entry probe are also presented to demonstrate the capabilities of FIAT.

Governing Equations and Numerical Procedures

This section presents a summary of the equations solved by FIAT and a discussion of some pertinent aspects of the numerical procedures.

Internal Energy Balance Equation

The internal energy balance is a transient thermal conduction equation with additional radiation and pyrolysis terms[2]

$$\rho c_p \left.\frac{\partial T}{\partial \theta}\right|_x = \frac{\partial}{\partial x}\left(k\frac{\partial T}{\partial x} - q_R\right)_\theta + (h_g - \bar{h})\left.\frac{\partial \rho}{\partial \theta}\right|_y + \dot{s}\rho c_p \left.\frac{\partial T}{\partial x}\right|_\theta + \dot{m}_g \left.\frac{\partial h_g}{\partial x}\right|_\theta \tag{1}$$

In Eq. (1) the x-coordinate system moves with the receding surface, whereas the y-coordinate system is stationary. The individual terms in Eq. (1) may be interpreted as follows: rate of storage of sensible energy, net rate of thermal conductive and radiative heat fluxes, pyrolysis energy-consumption rate, convection rate of sensible energy due to coordinate system movement, and net rate of energy convected by pyrolysis gas.

The radiative heat flux for a gray medium with isotropic scattering is[9]

$$\frac{q_R}{2\pi} = \int_0^1 i^+(0,\mu)\exp\left(\frac{-\kappa}{\mu}\right)\mu\,\mathrm{d}\mu - \int_0^1 i^-(\kappa_D,-\mu)\exp\left(\frac{\kappa_D-\kappa}{-\mu}\right)\mu\,\mathrm{d}\mu + \int_0^\kappa I'(\kappa^*)E_2(\kappa-\kappa^*)\,\mathrm{d}\kappa^* - \int_\kappa^{\kappa_D} I'(\kappa^*)E_2(\kappa^*-\kappa)\,\mathrm{d}\kappa^* \tag{2}$$

where κ is the optical thickness, $I'(\kappa^*) = \sigma T^4/\pi$ for radiative equilibrium conditions, and E_2 is the exponential integral function.[9] If the material is optically thick (opaque, $\kappa \to \infty$), which is true for some solids, Eq. (2) simplifies to

$$q_R = -\frac{4\sigma}{3(a+\sigma_s)}\frac{\partial T^4}{\partial x} \tag{3}$$

The local specific heat is formulated from functions of temperature input for both virgin material and char. In partially pyrolyzed zones ($\rho_c < \rho < \rho_v$), the specific heat is obtained from the mixing rule

$$c_p = \tau c_{pv} + (1-\tau)c_{pc} \tag{4}$$

where the weight variable τ is the mass fraction of virgin material in a mixture of virgin material and char that yields the correct local density:

$$\tau = (1-\rho_c/\rho)/(1-\rho_c/\rho_v) \tag{5}$$

The thermal conductivity k and extinction coefficient K are weighted in a similar manner. The pyrolysis gas enthalpy h_g is an input function of temperature and pressure. The quantity $\bar{h}$ is defined as

$$\bar{h} = \frac{\rho_v h_v - \rho_c h_c}{\rho_v - \rho_c} \tag{6}$$

Internal Decomposition Equation

A three-component decomposition model is used. The resin filler is presumed to consist of two components that decompose separately, whereas the reinforcing material is a third component that can decompose. The instantaneous density of the composite is given by

$$\rho = \Gamma(\rho_A + \rho_B) + (1-\Gamma)\rho_C \tag{7}$$

where subscripts A and B represent components of the resin and C represents the reinforcing material. Γ is the volume fraction of resin and is an input quantity. Each of the three components can decompose following the relation

$$\left.\frac{\partial \rho_i}{\partial \theta}\right|_y = -B_i e^{-E_i/T}\rho_{vi}\left(\frac{\rho_i - \rho_{ci}}{\rho_{vi}}\right)^{\Psi_i}, \qquad i = A, B, C \tag{8}$$

where ρ_{vi} and ρ_{ci} are the original and residual densities of component i, respectively.

Internal Mass Balance Equation

Internal decomposition converts some of the solid into pyrolysis gas. Assuming quasisteady one-dimensional flow and an impermeable backface, the pyrolysis gas mass flux is related to the decomposition by the simple mass balance[5]

$$\frac{\partial \dot{m}_g}{\partial y} = \frac{\partial \rho}{\partial \theta} \tag{9}$$

Surface Energy Balance Equation

The conditions at the ablating surface are determined by convective and radiative heating and by thermochemical interactions of the surface with the hot boundary-layer gas. The surface energy balance equation employed is of the convective transfer coefficient type and takes the following form[2]:

$$\rho_e u_e C_H(H_r - h_{ew}) + \dot{m}_c h_c + \dot{m}_g h_g + \rho_e u_e C_M\left[\sum\left(Z^*_{je} - Z^*_{jw}\right)h_j^{T_w} - B' h_w\right] + \alpha_w q_{rw} - F\sigma\varepsilon_w T_w^4 - q_{cw} = 0 \tag{10}$$

The first term in Eq. (10) represents the sensible convective heat flux. The sum of the second, third, and fourth terms is defined as the total chemical energy at the surface. The Z^* terms represent transport of chemical energy associated with chemical reactions at the wall and in the boundary layer.[10] The Z^* driving force for diffusive mass transfer includes the effects of unequal diffusion coefficients. The fifth and sixth terms are the radiative heat fluxes absorbed and reradiated by the wall, respectively, and the last term is the rate of conduction into the TPS.

A blowing correction allows for the reduction in transfer coefficient due to the transpiration effect of the mass injection into the boundary layer. The blowing rate correction for convective heat transfer is

$$\frac{C_H}{C_{H1}} = \frac{\ln(1+2\lambda B')}{2\lambda B'} \tag{11}$$

where λ is the blowing reduction parameter, C_H is heat transfer coefficient for the ablating surface, and C_{H1} is the heat transfer coefficient for a nonablating surface. With $\lambda = \frac{1}{2}$, Eq. (11) reduces to the classical laminar flow blowing correction.[11]

Numerical Procedures

The four main equations solved at each computational time step are the internal energy balance equation (1), the internal decomposition equation (8), the internal mass balance equation (9), and the surface energy balance equation (10). The internal energy balance equation is discretized using the finite volume method for each computational cell, and the internal decomposition is computed for each node. These equations are strongly coupled within the implicit scheme except for the radiative heat flux term defined in Eq. (2). The dependent variables in the discretized equations are T, q_c, ρ, g, and ρ_i $(i = A, B, C)$. The block matrix solver in the FIAT code is the same as that used in OMLITS.[12]

A fully implicit treatment of the radiation term in Eq. (2) would require the inversion of a full matrix, which is very computationally expensive. Instead, FIAT currently treats Eq. (2) as an explicit source term in Eq. (1). From our experience, radiation tends to reduce temperature gradients within the solid; thus, explicit treatment of Eq. (2) does not create an instability problem unless radiation within the solid is dominant, which is unlikely to occur in sizing computations of currently known TPS materials. An option for fully implicit treatment of Eq. (2) may be considered in a future version of FIAT if necessary. For an optically thick medium, the radiative flux term of Eq. (3) is used instead of Eq. (2), and this term is coded implicitly within Eq. (1). The matrix system remains block tridiagonal because radiation transport through an opaque medium depends only on conditions at neighboring nodes.

Surface thermochemistry tables required for solution of the surface energy balance equation (10), are computed by the program ACE[10] or the program MAT.[13] The user selects sets of values for pressure P, dimensionless gas rate B'_g, and dimensionless char rate B'_c; specifies the elemental composition of the environmental gas, the char, and the pyrolysis gas; and supplies thermodynamic data for all species in the system. The thermochemistry code then computes all of the dependent quantities of interest at each table point in the $P \times B'_c \times B'_g$ matrix of independent variables.

For problems with ablation, the computational grid is compressed to reflect the surface recession at each time step. The size of the compressed zone can be specified by the user. For the thermal response of nonablating heatshield materials, FIAT performs just like OMLITS because the nonablating surface is merely a special case of the general ablating surface condition.

Two input files are required for running the FIAT code. The first file contains all material properties including pressure-dependent thermal conductivity, specific heat, emissivity, absorptivity, decomposition kinetics, pyrolysis gas enthalpy, and thermochemistry tables. An index is assigned to each TPS material or structure listed in this file, and FIAT searches for material properties based on the assigned index. The material property file can be directly generated from the material database program TPSX[14] and reused for different applications without modification. The second input file, which is application dependent, specifies the control parameters, the heating environment, and the computational grid. The convective heating environment can be specified using an enthalpy or temperature heat transfer coefficient or a prescribed heat flux.[15]

An optimized TPS material thickness can be computed through a global iteration loop using a shooting method. The maximum bondline temperature and the convergence criterion are defined by the user. The FIAT code also provides interfaces with flow codes, such as GIANTS[16] and GASP,[17] and with thermochemistry codes, such as MAT and ACE, for high-fidelity fully coupled TPS sizing computation. Examples of such coupled sizing computations are presented in separate papers.[3,4]

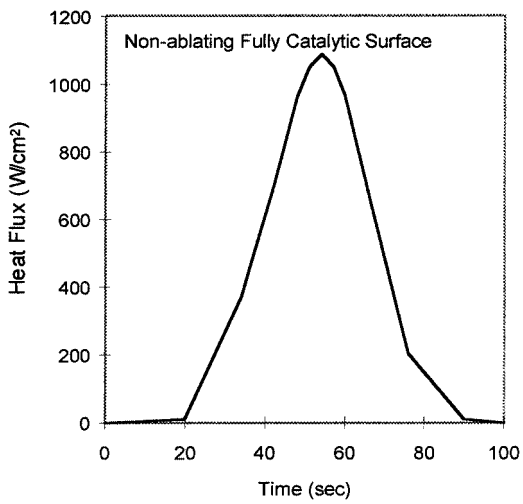

Fig. 1a Surface heating history at the stagnation point of the Stardust forebody.

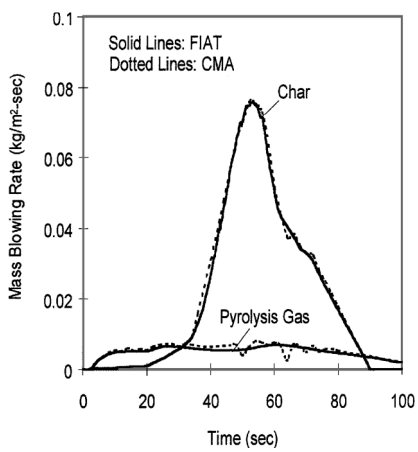

Fig. 1b PICA mass blowing rate history for total heat load of 27 kJ/cm^2.

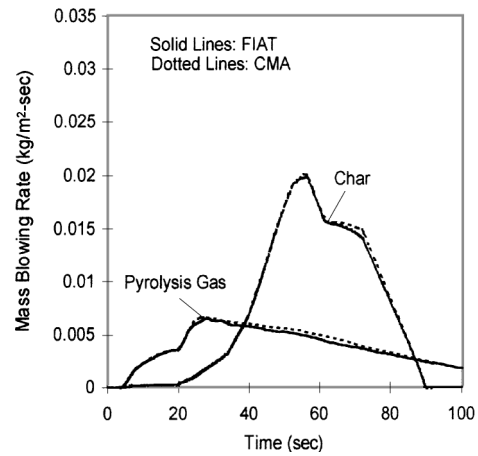

Fig. 1c PICA mass blowing rate history for total heat load of 13.5 kJ/cm^2.

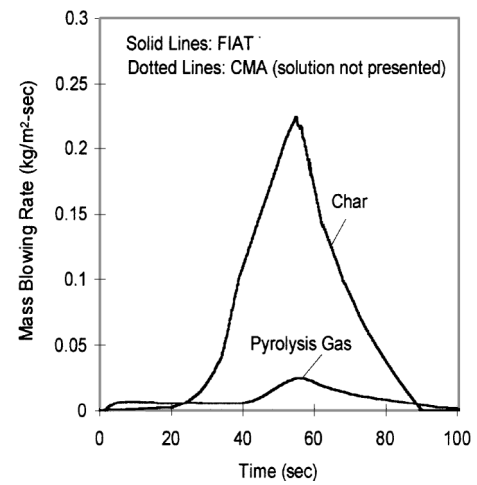

Fig. 1d PICA mass blowing rate history for total heat load of 54 kJ/cm^2.

Results and Discussion

In the first part of this section, comparisons between FIAT and CMA solutions are presented to demonstrate the difference in performance between the two codes and also to check the code consistency. In the second part, the thermal response of PICA and SIRCA under arcjet conditions (as predicted by FIAT) are shown and compared with thermocouple data. In the last part, the applications of FIAT for flight conditions, including the Stardust, Saturn Entry Probe, Mars 2001, and Mars Microprobe missions, are demonstrated. Most of these flight cases cannot be easily solved using the CMA code because of the numerical instability problem discussed earlier.

The effect of radiation on the performance of TPS materials can be an important issue. However, because there is insufficient experimental data to support the computational work, radiation effects are not included in this paper, but will be examined in the future.

Code Comparison

The mass blowing rates of char and pyrolysis gas of a PICA heatshield surface for a proposed Stardust trajectory have been computed using both FIAT and CMA. The nonablating fully catalytic surface heating history[4] is shown in Fig. 1a. The total heat load is approximately 27 kJ/cm^2. A comparison of predictions between the two codes is presented in Fig. 1b. The solid lines are the FIAT solution and the dotted lines are the CMA solution. In general, the predicted mass blowing rates are in good agreement except for the oscillations seen in the CMA solution. It has been found that the magnitude and location of these oscillations depend on the time step and grid selected by the user. For some combinations of time step and grid, a converged CMA solution can be obtained with some degree of oscillation, but for other combinations the oscillations become so severe that no converged solution is obtained.

Because of the matrix operations in the implicit solution, the computer time required for FIAT is approximately 35% more than that for CMA to complete one time step. This difference may vary as the grid size or heating rate changes. No attempt was made to highly optimize the FIAT code because the total computing time for a typical FIAT run is only a few seconds on a modern desktop workstation.

If the total heat load is halved (to 13.5 kJ/cm^2), the predicted mass blowing rates from both codes decrease, as shown in Fig. 1c. For this relatively low heat load case, no oscillation appears in the CMA solution, and the two solutions are almost on top of each other. If the total heat load is doubled (to 54 kJ/cm^2), the blowing rates increase as shown in Fig. 1d. For this high heat load condition, no converged CMA solution was obtained, and only the FIAT solution is presented. The average and maximum percent difference in surface blowing rates between FIAT and CMA solutions is listed in Table 1. The average difference is less than 2% for the relatively smooth solutions at 13.5 kJ/cm^2 (Fig. 1c) and 3–9% for the oscillatory solutions at 27 kJ/cm^2 (Fig. 1b).

This example shows that if the total heat load is low, nearly identical solutions can be computed successfully using either the explicit (CMA) or implicit (FIAT) code. If the heat load is about the level

Table 1 Difference between FIAT and CMA solutions

		Solution difference,[a] %	
Case	Mass flux	Average	Maximum
13.5 kJ/cm^2	Char	1.2	3.9
	Pyrolysis	1.7	6.0
27.0 kJ/cm^2	Char	3.8	12.3
	Pyrolysis	8.9	31.8

[a]Solution difference = abs[(FIAT-CMA)/FIAT].

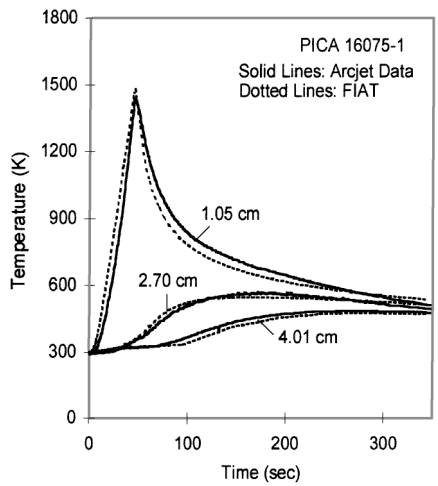

a) PICA run 16075-1

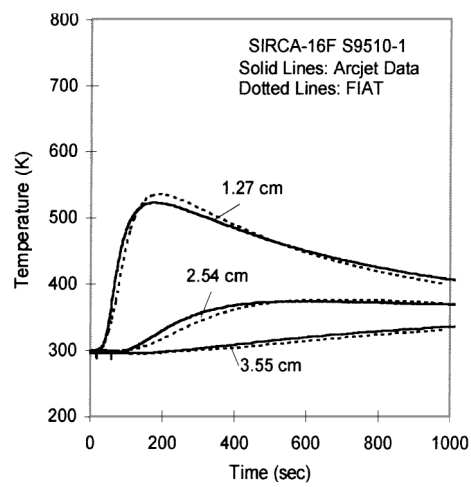

c) SIRCA run S9510-1

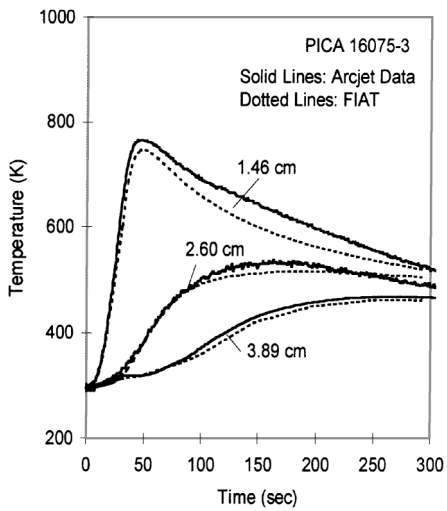

b) PICA run 16075-3

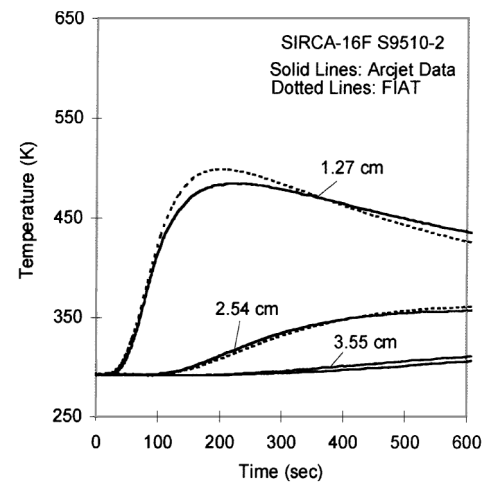

d) SIRCA run S9510-2

Fig. 2 Comparison between FIAT solution and arcjet thermocouple data; labels indicate thermocouple depth.

of that at the forebody stagnation point of the Stardust aeroshell, the explicit solution can be obtained with some oscillations, but the quality of solution is sensitive to the selected time step and grid. If the heat load is further increased, explicit solutions are difficult to obtain. The results from this test case demonstrate that FIAT is numerically more stable and solves a wider range of problems compared with CMA.

Arcjet Simulation

In Figs. 2a–2d, the in-depth thermal responses of PICA and SIRCA predicted by the FIAT code are compared with arcjet thermocouple data. The arcjet tests were conducted in the NASA Ames 60 MW Interactive Heating Facility and 20 MW Aerothermal Heating Facility. The test models were flat-faced cylinders with diameters ranging from 13.97 to 15.24 cm. Three thermocouples were installed at different depths in each test model. Details of the arcjet testing can be found in Refs. 6 and 7. The purpose of the FIAT analysis was to develop and validate material response models for these materials over a range of heating conditions. The in-depth thermal response was assumed to be one dimensional near the model axis, where the thermocouples were located.

Many arcjet test cases for each material have been computed and compared with thermocouple data. However, because of space limitations, only two representative cases for each material are presented here. The arcjet conditions for the four cases are listed in Table 2. The temperature histories of PICA at three depths for models 16075-1 and 16075-3 are shown in Figs. 2a and 2b, respectively. The surface recession for model 16075-1 is 0.69 cm and that for model 16075-3 is 0.48 cm. The solid lines are the thermocouple data, and the dotted lines are the FIAT predictions. The FIAT calculations provided a reasonable match to the in-depth thermocouple data as well as to the surface temperature and recession. The temperature histories of SIRCA for models S9510-1 and S9510-2 are shown in Figs. 2c and 2d, respectively. The surface recession for model S9510-1 is 0.09 cm and that for model S9510-2 is 0.03 cm. The SIRCA total surface recession for these test conditions was sufficiently small so that surface recession could be ignored, and only internal decomposition (pyrolysis) was considered in the FIAT computations.

Flight Applications

Stardust

PICA was selected as the Stardust forebody TPS material. Predictions of PICA thermal response were obtained using the FIAT code, and representative solutions are presented in Figs. 3a–3d. The Stardust forebody aeroshell is a 60-deg half-angle sphere-cone with nose radius of 0.23 m and base radius of 0.41 m. The convective and radiative heating of a nonablating fully catalytic surface at seven trajectory points were obtained by Olynick et al.[4] using the GIANTS and NOVAR codes.[18] The thermal response of PICA is assumed to be one dimensional. This assumption is true for most of the forebody surface except near the corner. The total integrated heat load over the forebody surface with blowing reduction parameter of 0.5 is shown in Fig. 3a. The heat load at the stagnation point is about 27 kJ/cm^2. The maximum contribution from radiation is about 2 kJ/cm^2 (7.5% of the total heat load).

Table 2 Summary of arcjet test conditions[6,7]

Material	$q_{\text{cold wall}}$, W/cm^2-s	Model no.	Stagnation pressure, atm	Test time, s	Recession, cm	
					Arcjet	FIAT
PICA	568	16075-1	0.28	45	0.69	0.64
PICA	852	16075-3	0.34	30	0.48	0.45
SIRCA-15F	50	S9510-1	0.20	60	0.09	0.00
SIRCA-15F	33	S9510-2	0.10	60	0.03	0.00

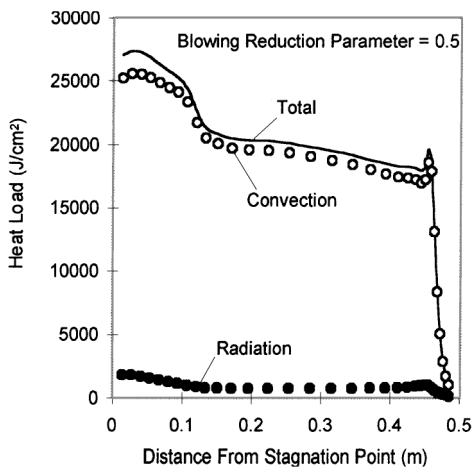

Fig. 3a Heat load distributions over the Stardust aeroshell forebody.

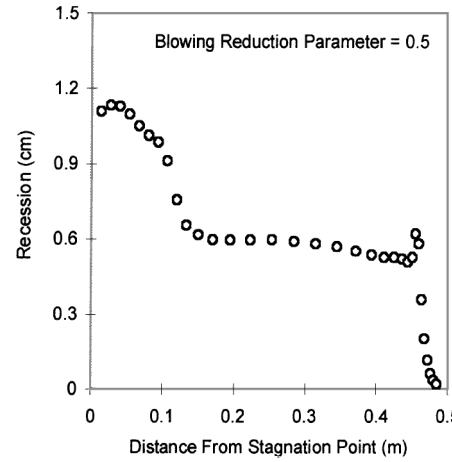

Fig. 3b Surface recession distribution over the Stardust aeroshell forebody.

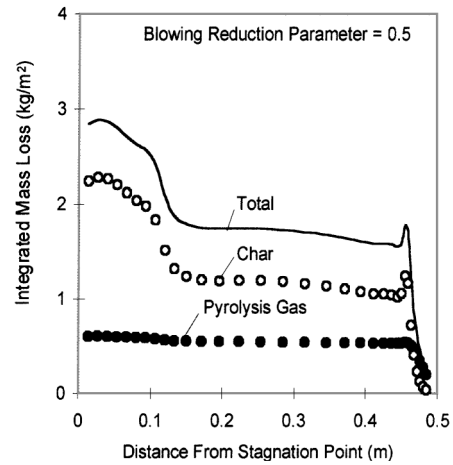

Fig. 3c Mass loss distributions over the Stardust aeroshell forebody.

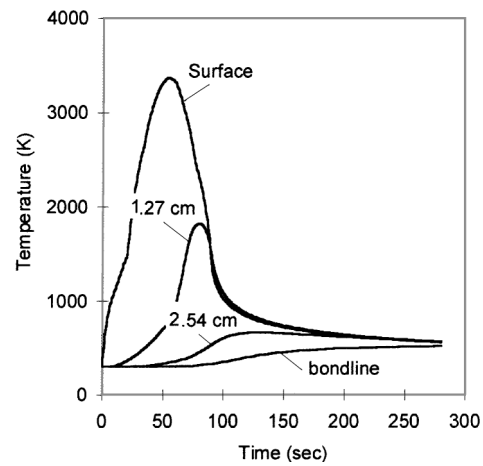

Fig. 3d Temperature histories at the stagnation point of the Stardust aeroshell.

The stagnation-pointmass blowing rate history is shown in Fig. 1a and was discussed earlier. In Fig. 3b, the surface recession distribution over the forebody surface is presented. The surface recession is 1.07 cm at the stagnation point, about 0.6 cm at the conical section, and 0.63 cm at the corner. The total mass loss, including char recession and pyrolysis gas, per unit area vs distance is shown in Fig. 3c. The total mass loss of PICA over the entire forebody surface is 1.06 kg. The temperature histories for the stagnation point at the ablating surface and at fixed depths of 1.27, 2.54, and 5.08 cm (the bondline) are presented in Fig. 3d. The maximum surface temperature is around 3400 K at the peak heating point. The heatshield thickness was optimized to maintain a bondline temperature below 523 K.

The FIAT solution presented here was not fully coupled with the flow environment code. The thermal response solution was obtained using the nonablating heat flux computed from the flow code with assumed blowing reduction parameter. A blowing reduction parameter $\lambda = \frac{1}{2}$ is used for all the Stardust results presented. A fully coupled computation[4] has also been performed using FIAT and GIANTS. The fully coupled solution showed that $\lambda = \frac{1}{2}$ is a good approximation in the vicinity of the stagnation point. Details of the fully coupled computations are discussed in Ref. 4 for Stardust and in Ref. 3 for Mars Pathfinder. The CMA code was used for the latter case in which the surface heating was low compared with the Stardust entry and the surface recession was negligibly small. Because of the numerical instability problem discussed earlier, the CMA code failed to perform the fully coupled iterations for the Stardust forebody computation.

Mars Microprobe (Deep Space II)

In Figs. 4a–4d, the thermal responses of Mars Microprobe forebody heatshield candidate materials predicted by the FIAT code are presented. The aeroshell of the Mars microprobe is a 45-deg half-angle sphere–cone. The nose radius is 6.2 cm, the corner radius is 1.9 cm, and the base radius is 12.4 cm. The nonablating fully catalytic convective heat flux at 11 trajectory points was obtained using the GIANTS code.[3] The stagnation-point heating history is shown in Fig. 4a. The peak heating rate is 250 W/cm^2, and the total nonablating heat load is about 8.7 kJ/cm^2.

To meet special requirements for this mission, the surface recession in the nosetip region should be kept as low as possible. Thus, PICA and SIRCA highly loaded with secondary impregnation of polymethyl methacrylate (PMMA) were proposed as candidate heatshield materials. The intent was to maximize the pyrolysis gas blowing rate so as to minimize the char surface recession.

Figures 4b and 4c present the mass blowing rate history and the in-depth temperature, respectively, at the stagnation point for both materials. For PICA/PMMA the maximum pyrolysis gas blowing rate is around 0.14 kg/m^2-s, which is about one order of magnitude higher than the char mass blowing rate. For SIRCA/PMMA the maximum pyrolysis gas blowing rate is 0.06 kg/m^2-s. The optimized heatshield thickness is 1.02 cm for PICA/PMMA and 0.76 cm for SIRCA/PMMA. The total char recession is 0.1 cm for PICA/PMMA and 0.002 cm for SIRCA/PMMA. The surface temperature remains below 1700 K on PICA but reaches about 2200 K on SIRCA.

PMMA decomposes at relatively low temperature (about 673 K), and the carbon substrate of PICA has relatively high thermal conductivity. Sufficient thermal energy can be conducted into the pyrolyzing zone to support the large-scale PMMA decomposition in PICA. On the other hand, SIRCA has a lower thermal conductivity;

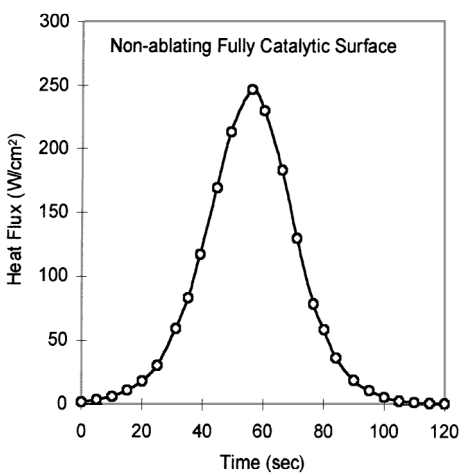

Fig. 4a Surface heating history at the stagnation point of the Mars microprobe.

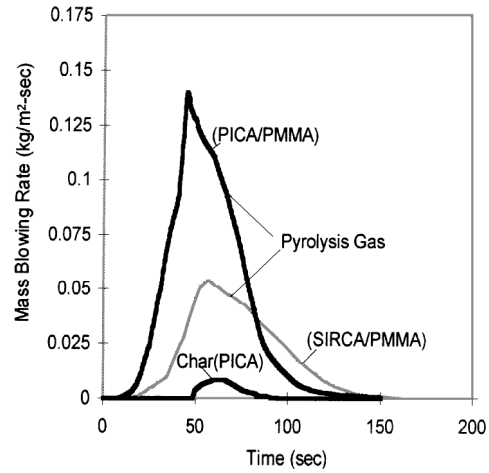

Fig. 4b Surface mass blowing rate history at the stagnation point of the Mars microprobe.

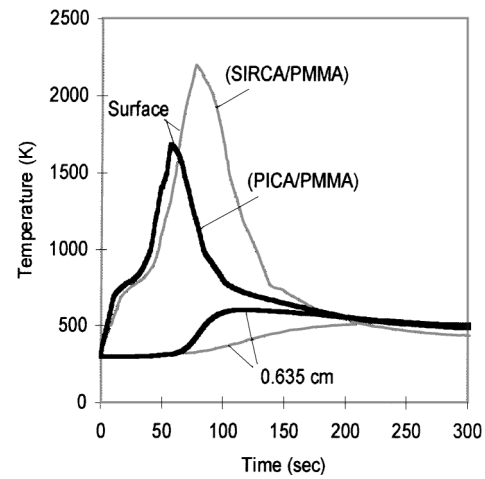

Fig. 4c Temperature histories at the stagnation point of the Mars microprobe.

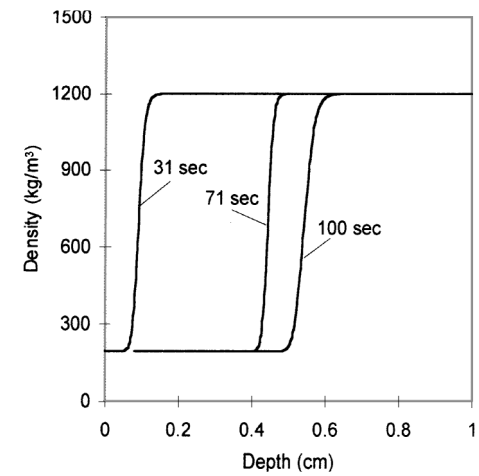

Fig. 4d In-depth density profiles at the stagnation point of the Mars microprobe.

thus, its pyrolysis rate is less than that of PICA, but its surface temperature is higher. Nevertheless, because of the long time for thermal soak for this mission (the heatshield remains attached until the vehicle impacts the surface), the higher conductivity material (PICA) has a larger optimized thickness.

The in-depth density profiles for PICA/PMMA at times of 31, 71, and 100 s are shown in Fig. 4d. The PMMA decomposes at such a high rate that the pyrolysis (density) front is very sharp. A fine spatial grid and small time step are required to accurately solve this problem.

Saturn Entry Probe

The TPS sizing for a proposed Saturn Entry Probe is presented in Figs. 5a–5d. Two TPS materials selected for this preliminary sizing were PICA-15 (240 kg/m^3) and conventional carbon phenolic (1440 kg/m^3). Results are presented for two different proposed trajectories that provide bounds for the heating environment. Trajectory 1 has entry velocity of 27 km/s and entry angle of −20 deg, whereas trajectory 2 has entry velocity of 30 km/s and entry angle of −45 deg. The probe forebody is a 45-deg half-angle sphere–cone, with nose radius of 26.25 cm and base radius of 46.8 cm.

Figure 5a shows the estimated nonablating surface heating distributions along the heatshield forebody surface for both trajectories. The optimized thickness and surface recession are shown in Figs. 5b and 5c, respectively. For this sizing calculation, the maximum bondline temperature is 560 K, and the heatshield is ejected at 151 s. The backface of TPS material is assumed to be adiabatic, and the blowing reduction parameter is assumed to be 0.5 for laminar flow and 0.35 for transitional and turbulent flow. The estimated total TPS mass is given in Fig. 5d. The total mass of carbon phenolic is about 32 kg for both trajectories, whereas the mass for PICA-15 is only about 7 kg.

This computation suggests that significant mass reduction can be achieved by using the newly developed lightweight ceramic ablative materials for the TPS on outer planetary entry probes. However, the strength of these materials must be assessed for such applications. Additionally, because the surface recession for PICA-15 is greater than that of carbon phenolic as the result of the density difference between the two materials, the effect of surface recession on aerodynamic performance should be studied if PICA is selected as the heatshield material.

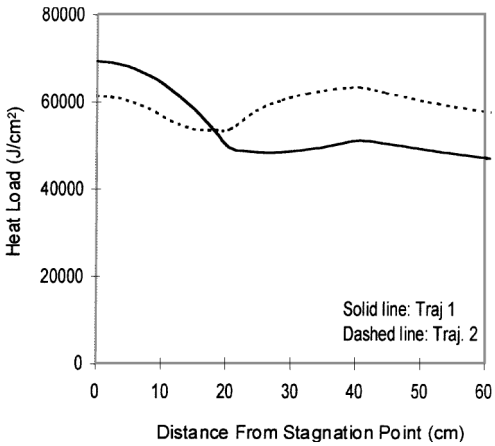

Fig. 5a Nonablating heat load distributions for the Saturn entry probe.

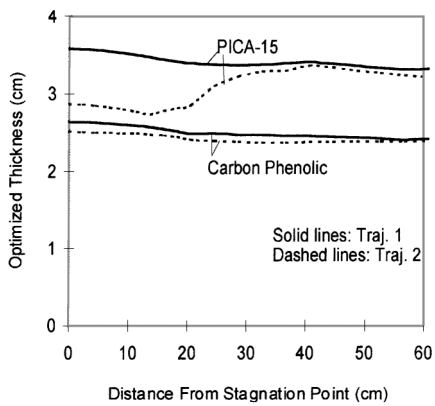

Fig. 5b Optimized thickness distributions for the Saturn entry probe.

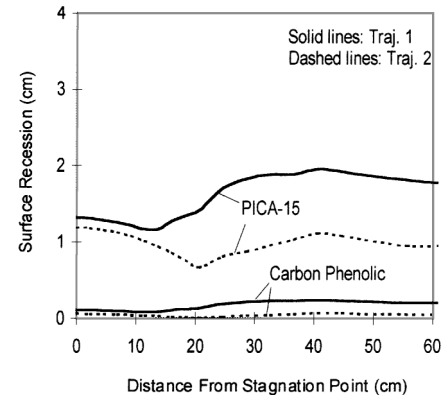

Fig. 5c Surface recession distributions for the Saturn entry probe.

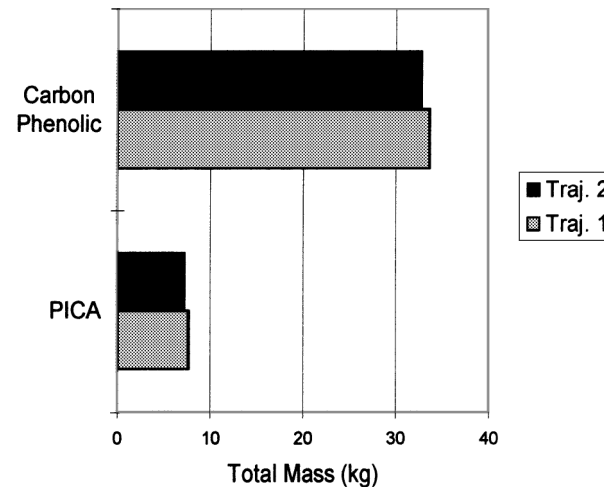

Fig. 5d Total TPS mass for the Saturn entry probe.

Mars 2001

The TPS sizing computation for the Mars 2001 heatshield is shown in Figs. 6a–6d. The Mars 2001 aerocapture vehicle is a 70-deg half-angle sphere–cone with nose radius of 0.60 m and corner radius of 0.06 m. A constant 11.1-deg angle of attack is assumed in the flow computation. A three-dimensional flow simulation was performed by Wercinski et al.[8] using the GASP code.[17] The integrated heat load along the pitch plane is shown in Fig. 6a. The maximum heat load occurs at the windward-side corner. The heat pulse is not high enough for significant surface recession to occur. Hence, computations were performed without surface recession but including in-depth pyrolysis. Three TPS materials [SIRCA-15F, SIRCA–secondary polymer-layered impregnated tile (SPLIT), and SLA-561V] were investigated for the preliminary sizing computation. SIRCA–SPLIT was modeled as a standard tile substrate with its outer half impregnated with RTV-556 resin, i.e., regular SIRCA, and the inner half impregnated with PMMA resin to the same total density.

The optimized thickness distributions along pitch plane for three materials are presented in Fig. 6b. The maximum thickness for SIRCA–SPLIT is about 3.1 cm, and that of SIRCA is about 3.4 cm. The thickness of SLA-561V is slightly higher than that of SIRCA. Figure 6c shows the stagnation point mass blowing rates for SIRCA and SIRCA–SPLIT to explain the difference in performance between two materials. The regular SIRCA has its peak mass blowing rate near the peak heating point (110 s), and then the blowing rate gradually declines. The pyrolysis gas blowing rate of SIRCA–SPLIT

has two peaks. The first peak, which is the same as that of a regular SIRCA, is due to the decomposition of RTV-556, and the second peak is the result of PMMA decomposition, which occurs as the thermal energy reaches the second-half of material. The high pyrolysis gas blowing rate blocks more surface convective heating, and additional energy is consumed in depth by the PMMA decomposition reactions. Consequently, SIRCA–SPLIT remains relatively cool in depth compared with regular SIRCA, and the optimized thickness of SIRCA–SPLIT is less than that of SIRCA. Figure 6d

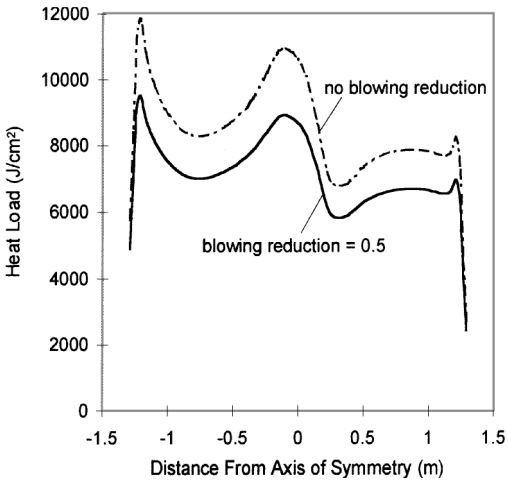

Fig. 6a Total heat load distributions over the Mars 2001 forebody pitch plane.

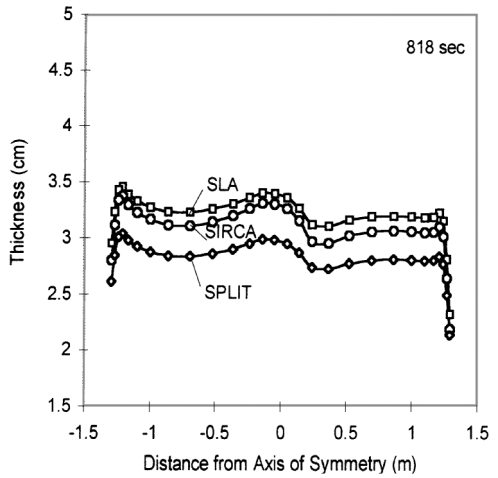

Fig. 6b Optimized TPS thickness distributions over the Mars 2001 forebody pitch plane.

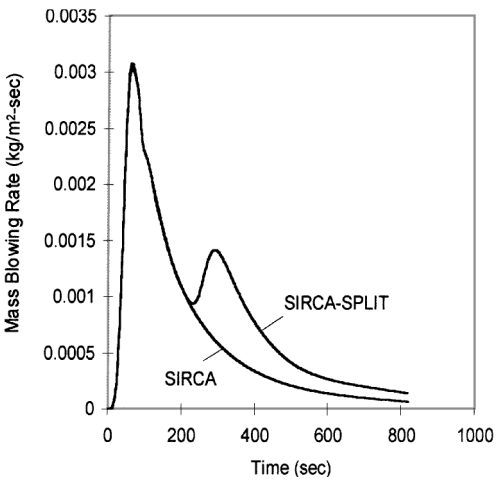

Fig. 6c Comparison of stagnation point mass blowing rates for the Mars 2001 heatshield.

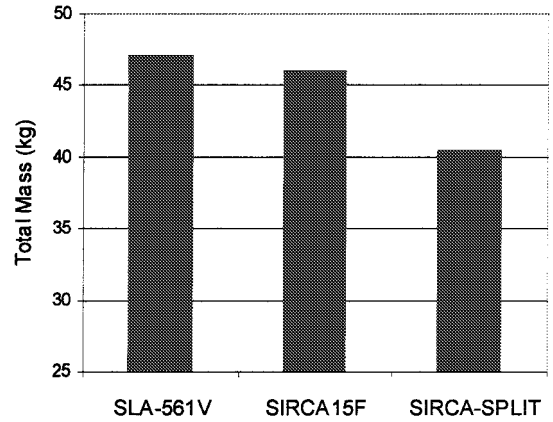

Fig. 6d Total TPS mass for the Mars 2001 aeroshell.

gives the total TPS mass for contoured aeroshells with optimized thickness distributions from Fig. 6b. The SIRCA–SPLIT material provides 5–6 kg of mass reduction compared with the other two materials. A comparable mass reduction is obtained for constant thickness aeroshells using the maximum thicknesses from Fig. 6b.

Conclusions

The FIAT program has been developed. FIAT solutions have been compared with arcjet thermocouple data and with solutions from the CMA code. The FIAT code was shown to be numerically more stable than CMA and, thus, capable of solving a wider range of problems. The application of FIAT for TPS thermal response and sizing for real flight missions, including the Stardust, Mars Microprobe, MARS 2001, and a Saturn Entry Probe with various TPS materials was demonstrated. FIAT has been proven to be an extremely useful computational tool for analysis and sizing of spacecraft heatshields.

Acknowledgment

This work was partially supported by NASA Ames Research Center under Contract NAS2-14031 to Eloret Thermosciences Institute.

References

[1] Moyer, C. B., and Rindal, R. A., "An Analysis of the Coupled Chemically Reacting Boundary Layer and Charring Ablator, Part II, Finite Difference Solution for the In-Depth Response of Charring Materials Considering Surface Chemical and Energy Balances," NASA CR-1061, June 1968.

[2] "User's Manual: Aerotherm Charring Material Thermal Response and Ablation Program," Aerotherm Div., Acurex Corp., Mountain View, CA, Aug. 1987.

[3] Chen, Y.-K., Henline, W. D., and Tauber, M. E., "Mars Pathfinder Trajectory Based Heating and Ablation Calculations," *Journal of Spacecraft and Rockets*, Vol. 32, No. 2, 1995, pp. 225–230.

[4] Olynick, D. R., Chen, Y.-K., and Tauber, M. E., "Forebody TPS Sizing with Radiation and Ablation for the Stardust Sample Return Capsule," AIAA Paper 97-2474, June 1997.

[5] Chen, Y.-K., and Milos, F. S., "Fully Implicit Ablation and Thermal Analysis Program (FIAT)," *ICCE/4, Fourth International Conference on Composites Engineering*, edited by D. Hui, International Community for Composites Engineering and College of Engineering, Univ. of New Orleans, New Orleans, LA, 1997, pp. 661, 662.

[6] Tran, H., Johnson, C., Rasky, D., Hui, F., Chen, Y.-K., and Hsu, M., "Phenolic Impregnated Carbon Ablators (PICA) for Discovery Class Missions," AIAA Paper 96-1911, June 1996.

[7] Tran, H., Johnson, C., Rasky, D., Hui, F., and Hsu, M., "Silicone Impregnated Reusable Ceramic Ablators for Mars Follow-on Missions," AIAA Paper 96-1819, June 1996.

[8] Wercinski, P. F., Papadopoulos, P., Milos, F., Venkapathy, E., Chen, Y.-K., Henline, W., and Tran, H., "Trajectory, Aerothermal Conditions, and Thermal Protection System Mass for the Mars 2001 Aerocapture Mission," AIAA Paper 97-0472, Jan. 1997.

[9] Siegel, R., and Howell, J. R., *Thermal Radiation Heat Transfer*, 2nd ed., McGraw–Hill, New York, 1981, pp. 471, 472.

[10] "User's Manual: Aerotherm Chemical Equilibrium Computer Program," Aerotherm Div., Acurex Corp., Mountain View, CA, Aug. 1981.

[11] Kays, W. M., and Crawford, M. E., *Convective Heat and Mass Transfer*, 2nd ed., McGraw–Hill, New York, 1980, pp. 353–361.

[12] Milos, F. S., Chen, Y.-K., and Henline, W. D., "Methodology for

Full-Body TPS Sizing of Access-to-Space Vehicles," AIAA Paper 96-0614, Jan. 1996.

[13]Milos, F. S., and Chen, Y.-K., "Comprehensive Model for Multi-Component Ablation Thermochemistry," AIAA Paper 97-0141, Jan. 1997.

[14]Squire, T. H., Milos, F. S., Hartlieb, G. C., and Rasky, D. J., "TPSX: Thermal Protection Systems Expert and Material Property Database," *ICCE/4, Fourth International Conference on Composites Engineering*, International Community for Composites Engineering and College of Engineering, Univ. of New Orleans, New Orleans, LA, 1997, pp. 937, 938.

[15]Chen, Y.-K., and Milos, F. S., "Solution Strategy for Thermal Response of Non-Ablating Thermal Protection System Materials at Hypersonic Speeds," AIAA Paper 96-0615, Jan. 1996.

[16]Chen, Y.-K., Henline, W. D., Stewart, D. A., and Candler, G. V., "Navier–Stokes Solutions with Surface Catalysis for Martian Atmospheric Entry," *Journal of Spacecraft and Rockets*, Vol. 30, No. 1, 1993, pp. 32–42.

[17]McGrory, D. M., Stack, D. C., Applebaum, M. P., and Walters, R. W., "GASP Version 2.2 User's Manual," Aerosoft, Inc., Blacksburg, VA, 1993.

[18]Olynick, D. R., Henline, W. D., Chambers, L. H., and Candler, G. V., "Comparison of Coupled Radiative Navier–Stokes Flow Solutions with the Project Fire II Flight Data," AIAA Paper 94-1955, June 1994.

R. D. Braun
Guest Editor